Striking similarity of ferroelectric aging effect in tetragonal, orthorhombic and rhombohedral crystal structures

Zuyong Feng and Xiaobing Ren
Ferroic Physics Group, National Institute of Materials Science, Tsukuba, 305-0047 Ibaraki, Japan
(Received 4 January 2008; revised manuscript received 10 March 2008; published 30 April 2008)

A series of Mn-doped alkaline niobate-based and lead zirconic titanate ferroelectrics that possess tetragonal, orthorhombic, and rhombohedral perovskite structures was fabricated, and the aging behavior of their hysteresis loop and electrostrain was studied. We found that after aging, all the samples showed a similar double hysteresis loop and large recoverable electrostrain behavior, regardless of their crystal structure and of their ionic species. The striking similarity of the aging effect in different ferroelectric phases suggests that there exists a common physical origin of aging in ferroelectric perovskites. Based on a symmetry-conforming short-range ordering mechanism of point defects, we provided a unified microscopic explanation for the aging effect in the tetragonal, orthorhombic, and rhombohedral ferroelectrics.

DOI: 10.1103/PhysRevB.77.134115 PACS number(s): 77.80.Dj, 77.84.Dy, 61.72.−y

I. INTRODUCTION

Aging phenomenon, a time-dependent change in ferroelectric, dielectric, and piezoelectric properties, has been observed in many ferroelectrics.[1–4] After aging, ferroelectrics often show an abnormal double (or constricted) polarization-electric field (*P-E*) hysteresis loop.[5–13] Aging strongly affects the application of ferroelectrics, especially the reliability of ferroelectric and dielectric devices. Recent studies have also shown that aging can also generate a large electrostrain effect due to a reversible domain switching mechanism.[8–13] Therefore, ferroelectric aging is an issue of both fundamental and practical importance, and this is why it has drawn much attention over the past decades.[1–17]

Historically, quite a number of models, such as grain-boundary model,[2,18,19] domain-wall pinning model,[5] and volume effect model,[6,20,21] have been proposed to explain the origin of aging. Experiments using single crystal samples suggest that grain boundary effect is not a primary origin of aging.[6,12] Thus, it is generally agreed that aging is attributed to a gradual stabilization of the ferroelectric domain structure by defects (dopant, vacancy, or impurity). However, the central controversy had been whether the domain stabilization stems from a domain-wall-pinning effect or a volume effect. For domain-wall-pinning effect, it is believed that defects migrate to the domain walls during aging and consequently pin the domain walls. Pinning effect may be a general mechanism, but it cannot explain the similar aging behavior in *single-domain* (domain-wall-free) Mn-doped $BaTiO_3$ single crystal.[6,12] As to volume effect, it is considered that during aging, the polar defects will align along the spontaneous-polarization ($\mathbf{P}_S$) direction over the whole domain and thus make domain switching difficult.[6] Recent studies suggest that the volume effect arises from a symmetry-conforming principle of point defects, which explains not only the aging in ferroelectrics[8–13] but also the aging in metallic martensite where no spontaneous polarization exists.[22,23]

Although ferroelectric aging phenomenon has been commonly observed in many tetragonal ferroelectrics (such as $BaTiO_3$), little is known about its dependence on crystal structure or symmetry of ferroelectrics. It is unclear whether there exists a similar aging effect and a common microscopic mechanism in all kinds of ferroelectrics, which does not depend on their crystal structure and ionic species. To answer this interesting question, in the present work, we fabricated a series of Mn-doped ferroelectric ceramics that possess tetragonal, orthorhombic, and rhombohedral perovskite structure; we made a systematic investigation on their aging behavior. As will be seen in the following, we found that after aging all the samples showed a strikingly similar double hysteresis loop and a large recoverable electrostrain behavior. The similar aging behavior for ferroelectrics of different crystal structures and/or symmetries and ionic species suggests a common mechanism of aging. Based on the symmetry-conforming short-range ordering (SC-SRO) principle of point defects,[8,9,13] we provide a unified microscopic explanation for aging in these different perovskite ferroelectrics.

II. EXPERIMENT

$(K_{0.98}Li_{0.02})[(Nb_{0.65}Ta_{0.35})_{0.99}Mn_{0.01}]O_3$ [abbreviated as $(KLi_{0.02})(NbTa_{0.35})O_3$-1Mn], $(K_{0.5}Na_{0.5})(Nb_{0.99}Mn_{0.01})O_3$ (abbreviated as KNN-1Mn) and $Pb[(Zr_{0.58}Ti_{0.42})_{0.99}Mn_{0.01}]O_3$ (abbreviated as PZT58/42-1Mn) ceramics were chosen as our test samples, which were synthesized using the conventional solid-state reaction techniques.[3,13,24] The starting chemicals were high purity oxide or carbonate (>99.5%). $(KLi_{0.02})(NbTa_{0.35})O_3$-1Mn was calcined at 950 °C for 2 h in a K_2O-rich atmosphere and followed by sintering at 1125 °C for 0.5 h in air. Calcining of KNN-1Mn was done at 900 °C for 2 h in a K_2O- and Na_2O-rich atmosphere and followed by sintering at 1100 °C for 0.5 h in air. Calcining of PZT58/42-1Mn was done at 900 °C for 2 h in a Pb_2O-rich atmosphere, followed by sintering at 1125 °C for 2 h in a Pb_2O-rich N_2 atmosphere. Mn was added to *B* site as acceptor dopant. Its valence state can be adjusted from 2+ to 4+ when sintered at high temperature with different O_2 partial pressure.[6,25,26] Mn ions are mainly Mn^{4+} when sintered in air, and Mn^{3+} in N_2 atmosphere. Oxygen vacancies are simultaneously created by charge compensation when acceptor dopant Mn was doped to *B* site.[27] The

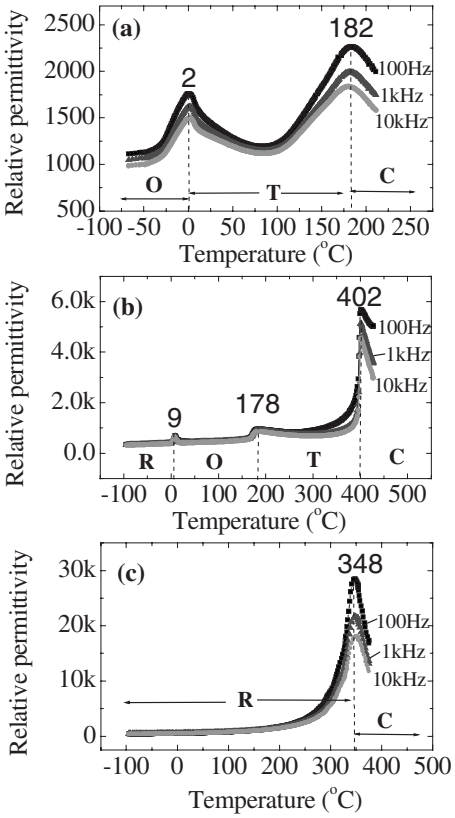

FIG. 1. Temperature dependence of the relative permittivity for (a) the tetragonal $(KLi_{0.02})(NbTa_{0.35})O_3$-1Mn, (b) orthorhombic KNN-1Mn, and (c) rhombohedral PZT58/42-1Mn ceramics, respectively, at frequency of 100 Hz, 1 kHz, and 10 kHz. C=cubic, T=tetragonal, O=orthorhombic, and R=rhombohedra.

relative permittivity as a function of temperature for the three samples is shown in Figs. 1(a)–1(c), respectively. The peaks signify the paraelectric-ferroelectric transition (cubic-tetragonal or cubic-rhombohedral) and ferroelectric-ferroelectric transition (tetragonal orthorhombic or orthorhombic rhombohedral), as indicated in Figs. 1(a)–1(c) XRD characterization indicates that $(KLi_{0.02})(NbTa_{0.35})O_3$-1Mn sample has a tetragonal structure throughout the whole temperature range from room temperature up to its T_C (182 °C); KNN-1Mn sample has an orthorhombic structure from room temperature up to 178 °C; PZT58/42-1Mn sample has a rhombohedral structure from room temperature to its T_C (348 °C). In order to establish a stable defect symmetry state, $(KLi_{0.02})(NbTa_{0.35})O_3$-1Mn sample was aged at 80 °C for two weeks, and KNN-1Mn and PZT58/42-1Mn were aged at 120 °C for two weeks. The *P-E* hysteresis loop and electrostrain were measured simultaneously using a Radiant Workstation and a MTI 2000 photonic sensor. During the measurement the testing sample was immersed in silicon oil, which can be set at any temperature between room temperature and 160 °C. The frequency of the measurement was fixed at 10 Hz.

III. RESULTS

Figure 2(a) shows a comparison in the *P-E* hysteresis loop and electrostrain for unaged and aged tetragonal $(KLi_{0.02})(NbTa_{0.35})O_3$-1Mn samples at room temperature. The variation of *P-E* hysteresis loop and electrostrain of the aged sample with temperature is shown in Fig. 2(b). For the unaged sample, when an electric field is applied, strain increases with increasing polarization. When the field decreases to zero, there is a remanent polarization due to the irreversible domain switching. This gives rise to the well-known normal hysteresis loop and irrecoverable butterfly-type electrostrain curve. Contrasting the unaged sample, the aged sample shows an abnormal double *P-E* hysteresis loop and a recoverable electrostrain behavior. That is, with an electric field increases to maximum, polarization and strain simultaneously increase to maximum. When the field drops to zero, the polarization and strain also becomes zero. The double hysteresis loop and a *recoverable* electrostrain curve for the aged tetragonal $(KLi_{0.02})(NbTa_{0.35})O_3$-1Mn sample is very similar to that of the aged acceptor-doped tetragonal $BaTiO_3$ ferroelectrics,[8–11] despite the different ionic species and valence ($A^+B^{5+}O_3$ for the former and $A^{2+}B^{4+}O_3$ for the latter). Therefore, aging effect seems not critically dependent on ionic species and valence. Figure 2(b) shows that the aging-induced double hysteresis loop and large recoverable electrostrain behavior can persist up to a high temperature even above 160 °C; this indicates a wide temperature range for the aging effect in tetragonal structure.

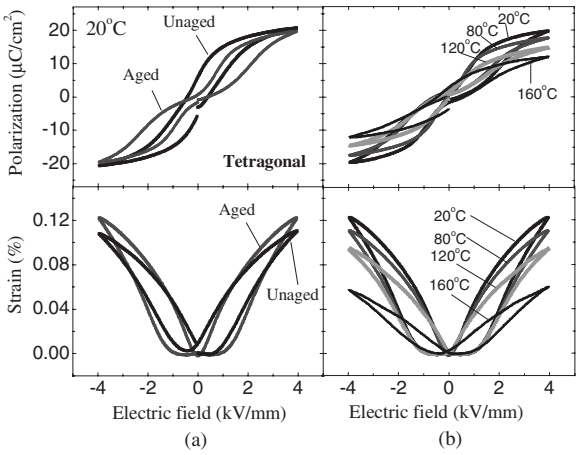

FIG. 2. (a) *P-E* hysteresis loop and electrostrain behavior for unaged and aged tetragonal $(KLi_{0.02})(NbTa_{0.35})O_3$-1Mn ceramics at room temperature. (b) The change in *P-E* hysteresis loop and electrostrain of aged tetragonal $(KLi_{0.02})(NbTa_{0.35})O_3$-1Mn ceramics with temperature.

Figures 3(a) and 4(a) show the *P-E* hysteresis loop and electrostrain for orthorhombic KNN-1Mn and rhombohedral PZT58/42-1Mn samples, respectively. The measurement was done at room temperature. The variation of *P-E* hysteresis loop and electrostrain of the two aged samples with temperature is shown in Figs. 3(b) and 4(b), respectively. In the past, little was known about the aging effect in orthorhombic and rhombohedral ferroelectrics. It is clear from Figs. 3 and 4 that both orthorhombic and rhombohedral samples exhibit a similar double hysteresis loop and recoverable electrostrain curve after aging, whereas the unaged state exhibits normal behavior. Moreover, the aging-induced double-hysteresis

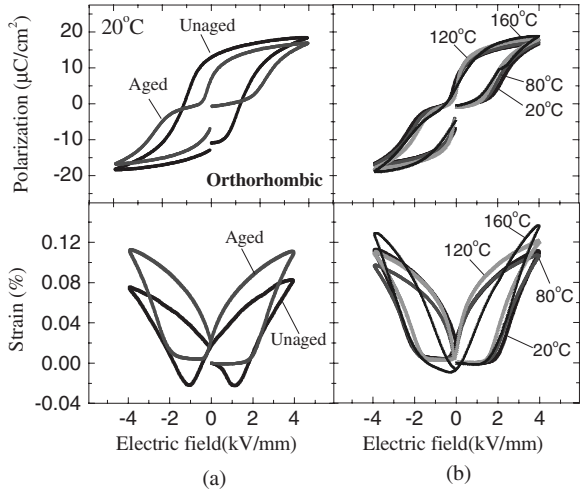

FIG. 3. (a) *P-E* hysteresis loop and electrostrain behavior for unaged and aged orthorhombic KNN-1Mn ceramics at room temperature. (b) The change in *P-E* hysteresis loop and electrostrain of aged orthorhombic KNN-1Mn ceramics with temperature.

loop and large recoverable electrostrain behavior of the two samples can also persist up to a high temperature even above 160 °C in the orthorhombic and rhombohedral phase, respectively, as shown in Figs. 3(b) and 4(b). Thus the less-known aging effect in orthorhombic and rhombohedral ferroelectrics turned out to be very similar to that in the familiar tetragonal ferroelectrics (Fig. 2).

IV. DISCUSSION

The strikingly similarity of the aging effect in the tetragonal, orthorhombic, and rhombohedral samples suggests the existence of a common physical origin of aging in perovskite ferroelectrics, which does not depend on crystal structure and/or symmetry and constituent ionic species. In the following, we will give a unified microscopic explanation for their similar aging effect based on the SC-SRO principle of point defects, which explained the similar effects in acceptor-doped $BaTiO_3$ ferroelectrics[8] and even in ferroelastic martensite.[22,23] The main idea is that point defects (i.e., acceptor ions and vacancies) tend to adopt a statistical symmetry that follows the crystal symmetry when in equilibrium (after aging); this stabilizes the existing domains and hence creates a restoring force for a reverse domain switching.

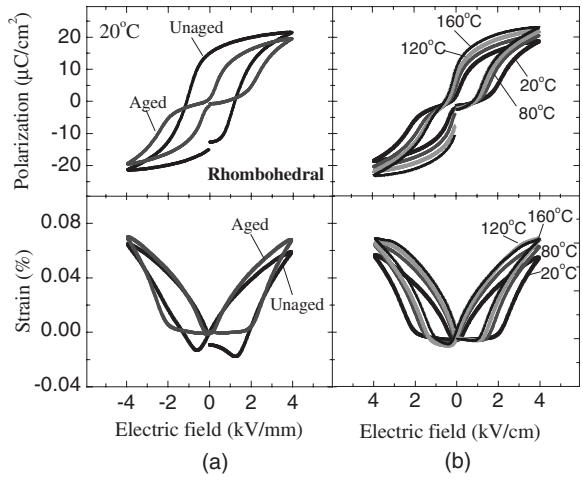

FIG. 4. (a) *P-E* hysteresis loop and electrostrain behavior for unaged and aged rhombohedral PZT58/42-1M ceramics at room temperature. (b) The change in *P-E* hysteresis loop and electrostrain of the aged rhombohedral PZT58/42-1Mn ceramics with temperature.

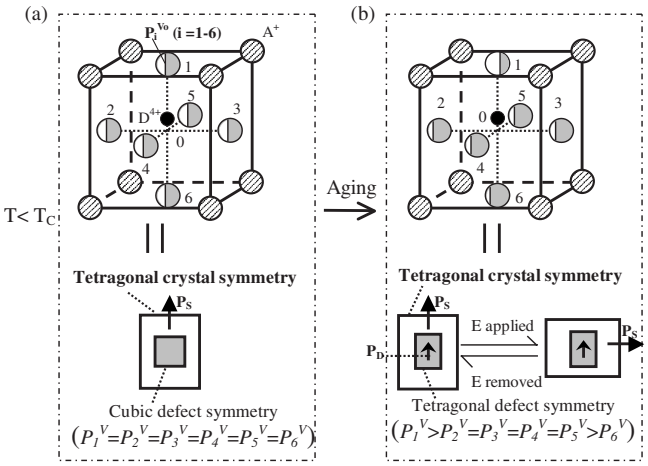

FIG. 5. Defect symmetry and tetragonal crystal symmetry in D^{4+}-doped tetragonal $A^+B^{5+}O_3$ structure. (a) unaged; (b) aged. $P_i^{V_O}$ is the conditional probability of oxygen vacancy occupying O^{2-} site i (i=1–6) next to a given D^{4+}. Large rectangle represents crystal symmetry and small rectangle represents defect symmetry. $\mathbf{P}_S$ refers to spontaneous polarization and $\mathbf{P}_D$ refers to defect polarization.

A. Microscopic explanation for the aging effect in tetragonal ferroelectrics based on the symmetry-conforming short-range ordering properties of point defects

Figure 5 presents the symmetry of statistical distribution of oxygen vacancies around an acceptor ion D^{4+} in a tetragonal perovskite $A^+B^{5+}O_3$ lattice [A^+=(K^+,Li^+), B^{5+}=(Nb^{5+},Ta^{5+})] for unaged [Fig. 3(a)] and well-aged [Fig. 3(b)] state, respectively. Doping acceptor D^{4+} at B^{5+} site will produce oxygen vacancies V_O at O^{2-} sites to maintain charge neutrality. In such a case D^{4+} dopants and O^{2-} vacancies as point defects. Usually these point defects are thought to distribute randomly; however, if we focus on the local (short-range) environment of a given defect D^{4+}, the short-range distribution of oxygen vacancies around it may show certain statistical symmetry.

For an unaged tetragonal sample, which is formed by immediately cooling from a cubic paraelectric state, the SRO distribution of point defects keeps the same cubic symmetry [Fig. 3(a)] as that in the cubic paraelectric phase, because the diffusionless paraelectric-ferroelectric transition cannot alter the original cubic SRO symmetry of point defects.[11] Thus, the defect (O^{2-} vacancy) probability P_i^V (i=1–6) around a given defect D remains the same at O^{2-} sites 1–6 (P_1^V=P_2^V=P_3^V=P_4^V=P_5^V=P_6^V), as being the case for a cubic phase. As a result, the unaged ferroelectric sample has a cu-

bic defect symmetry, which does not match the tetragonal crystal symmetry [see the bottom illustration of Fig. 5(a)]. According to the SC-SRO principle,[22,23] such a state is energetically unstable. This is because in a polar tetragonal structure, the six neighboring O^{2-} sites are not equivalent to the D^{4+} site: sites 2–5 are equivalent, but site 1 is closer and site 6 is farther in distance. It is natural that the closer site should have larger defect probability due to the Coulomb attractive force between the effectively negative D^{4+} dopant and the effectively positive O^{2-} vacancy. Therefore, a stable defect probability should be $P_1^V > P_2^V = P_3^V = P_4^V = P_5^V > P_6^V$, showing a polar tetragonal defect symmetry when in equilibrium. This stable state corresponds to the well-aged ferroelectric.

The difference in the stability of defect configuration between Figs. 5(a) and 5(b) create a driving force for a change in defect probabilities. Such a change involves a short-range migration of O^{2-} vacancies; thus, it requires some time to complete. This is the microscopic origin of the aging of the ferroelectric phase. Therefore, after aging for a long time in the ferroelectric state, defect symmetry gradually changes from cubic symmetry to a polar tetragonal one, following the polar tetragonal crystal symmetry, as shown in Fig. 3(b).

In the aged ferroelectrics, the polar tetragonal defect symmetry creates a defect polarization $\mathbf{P}_D$ aligning along the spontaneous polarization ($\mathbf{P}_S$) direction [see the bottom illustration of Fig. 5(b)]. When an electric field is applied to the aged tetragonal $A^+B^{5+}O_3$ sample, $\mathbf{P}_S$ is switched to the field $\mathbf{E}$ direction, but the defect symmetry and associated $\mathbf{P}_D$ cannot have a sudden change, as shown in the bottom illustration of Fig. 5(b). Therefore, after removing the electric field, the unchanged defect symmetry and the associated $\mathbf{P}_D$ provide an intrinsic restoring force to switch the $\mathbf{P}_S$ to its original orientation, thus causing a reversible domain switching. Macroscopically this reversible domain switching gives rise to a double-hysteresis loop and a large recoverable electrostrain behavior, as observed in Fig. 2.

Clearly, the explanation on aging effect of tetragonal acceptor-doped $A^+B^{5+}O_3$ sample is very similar to that of $A^{2+}B^{4+}O_3$ ferroelectrics.[8–11] That is, their aging originates from the inconformity of the defect symmetry with the crystal symmetry after a structural transition. This indicates that aging is not sensitive to the valence of the constituent ions.

B. Microscopic mechanism of the aging effect in orthorhombic ferroelectrics and rhombohedral ferroelectrics

Different from tetragonal ferroelectrics, orthorhombic ferroelectrics and rhombohedral ferroelectrics have a spontaneous polarization $\mathbf{P}_S$ along $\langle 110\rangle_{cub}$ and $\langle 111\rangle_{cub}$ direction, respectively. It is interesting to see how similar or how different their aging mechanisms are from that of the tetragonal ferroelectrics discussed above. Based on the SC-SRO properties of point defects, we show in the following that there exists a similar microscopic explanation for the aging effect in orthorhombic and rhombohedral ferroelectrics.

Figure 6 shows the symmetry of equilibrium statistical distribution of oxygen vacancies around an acceptor ion D^{4+} (or D^{3+}) in orthorhombic perovskite $A^+B^{5+}O_3$ lattice [A^+=(K^+,Na^+), B^{5+}=Nb^{5+}] for unaged [Fig. 6(a)] and well-aged [Fig. 6(b)] state, respectively. As the orthorhombic lattice can also be represented by a simpler monoclinic lattice,[3] as shown in Fig. 6, we shall use the monoclinic lattice throughout the discussion. With acceptor doping (D^{4+} for Nb^{5+} ions), oxygen vacancies V_O form to maintain charge neutrality. Following the same line of discussion as for the tetragonal ferroelectrics, we can make the same conclusion that for the unaged orthorhombic samples, which are formed by fast cooling down from the cubic paraelectric phase, the SRO distribution of point defects still keeps the same cubic symmetry [Fig. 6(a)] as that in the cubic paraelectric phase because fast cooling cannot alter the original cubic SRO symmetry of point defects. Thus, the defect (O^{2-} vacancy) probabilities P_i^V (i=1–6) are the same at the O^{2-} sites 1–6 ($P_1^V = P_2^V = P_3^V = P_4^V = P_5^V = P_6^V$). This means for the unaged ferroelectric state, cubic defect symmetry is inherited in the orthorhombic crystal symmetry [see the bottom illustration of Fig. 6(a)], and such two symmetries are not matching. According to the SC-SRO principle,[22,23] such a state is energetically unstable. It is noted that sites 1 and 4 are closest to the defect D^{4+}, sites 5 and 6 are next, and sites 2 and 3 are farthest. Following the same electrostatic energy consideration as discussed for the tetragonal case, one can readily deduce that the stable defect probability for an orthorhombic phase (with spontaneous polarization $\mathbf{P}_S$ along $\langle 110\rangle_{cub}$ direction) should be $P_1^V = P_4^V > P_5^V = P_6^V > P_2^V = P_3^V$, which has the same polar orthorhombic symmetry as its crystal symmetry, as shown in Fig. 6(b).

As the unaged orthorhombic state [Fig. 6(a)] is unstable, it tends to change into a stable state [Fig. 6(b)] through short-

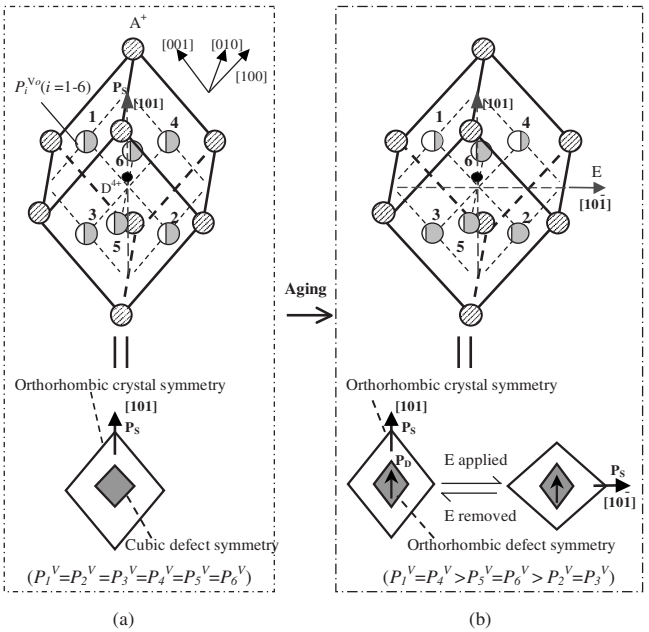

FIG. 6. Defect symmetry and orthorhombic crystal symmetry in D^{4+}-doped orthorhombic $A^+B^{5+}O_3$ structure: (a) unaged and (b) aged. $P_i^{V_O}$ is the conditional probability of oxygen vacancy occupying O^{2-} site i (i=1–6) next to a given D^{4+}. Large rhombus represents the projection of crystal symmetry and small rhombus represents the projection of defect symmetry. $\mathbf{P}_S$ refers to spontaneous polarization, and $\mathbf{P}_D$ refers to defect polarization.

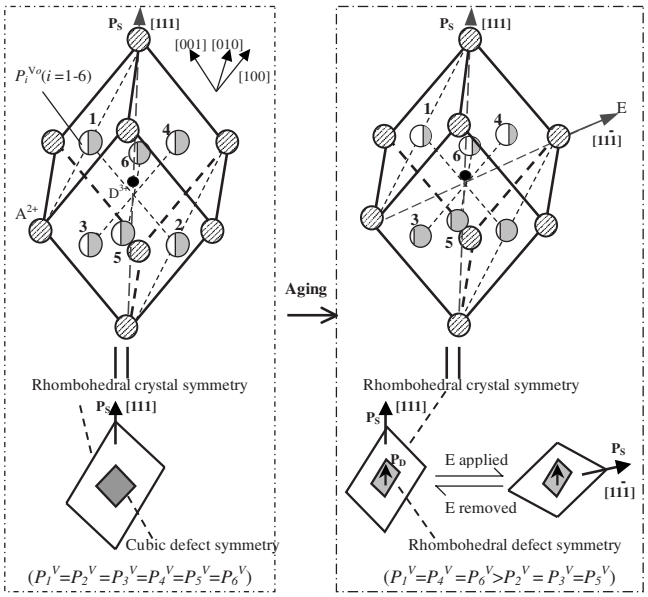

FIG. 7. Defect symmetry and rhombohedral crystal symmetry in D^{3+}-doped rhombohedral $A^{2+}B^{4+}O_3$ structure: (a) unaged and (b) aged. P_i^{Vo} is the conditional probability of oxygen vacancy occupying O^{2-} site i $(i=1-6)$ next to a given D^{3+}. Large parallelogram represents the projection of the rhombohedral crystal lattice and small parallelogram represents the projection of defect symmetry. $\mathbf{P}_S$ refers to spontaneous polarization and $\mathbf{P}_D$ refers to defect polarization.

range diffusion of oxygen vacancies. This is the origin of aging in the orthorhombic phase, being the same as the tetragonal case discussed above. The polar orthorhombic defect symmetry formed by acceptor Mn^{4+} dopants and O^{2-} vacancies makes a defect polarization $\mathbf{P}_D$ aligning along $\mathbf{P}_S$ direction $\langle 101\rangle_{cub}$ [Fig. 6(b)]. When an electric field is applied to an aged orthorhombic sample, as shown in Fig. 6(b), $\mathbf{P}_S$ orientation is changed to align along the electric field, but the defect symmetry and associated $\mathbf{P}_D$ cannot have a sudden change and is still in the original direction. Therefore, the unchanged defect symmetry and the associated $\mathbf{P}_D$ provide an intrinsic restoring force and cause a reversible domain switching such as the aforementioned tetragonal case. Consequently a macroscopic double-hysteresis loop and a large recoverable electrostrain behavior are achieved (Fig. 3). For the unaged samples, the defect symmetry has a cubic symmetry, which cannot provide a restoring force. This is why a normal macroscopic *P-E* hysteresis loop and butterfly-shape electrostrain curve is observed (Fig. 3). This is again similar to the unaged tetragonal ferroelectrics (Fig. 2). Therefore, aging in orthorhombic ferroelectrics has the same microscopic origin as that in tetragonal ferroelectrics, both are governed by the SC-SRO principle,

Following the same reasoning as that of the tetragonal phase and orthorhombic phase, we can show the aging effect of the rhombohedral ferroelectrics has a similar microscopic explanation due to the SC-SRO properties of point defects, as shown in Fig. 7. Figure 7 shows the symmetry of equilibrium statistical distribution of oxygen vacancies around an acceptor ion D^{3+} in rhombohedral perovskite $A^{2+}B^{4+}O_3$ lattice $[A^{2+}=Pb^{2+}, B^{4+}=(Ti^{4+},Zr^{4+})]$ for unaged [Fig. 7(a)] and well-aged [Fig. 7(b)] state, respectively. For rhombohedral ferroelectrics, its spontaneous polarization $\mathbf{P}_S$ is along $\langle 111\rangle_{cub}$ direction [Fig. 7(a)]. Acceptor ions (Mn^{3+}) substitute for central Ti^{4+} ions and create oxygen vacancies V_O. Following the same analysis as the tetragonal and orthorhombic cases with consideration of the rhombohedral crystal symmetry, we can conclude for the unaged ferroelectric the SRO distribution of point defects also inherits the same cubic symmetry as that in the cubic paraelectric phase because of the diffusionless paraelectric-ferroelectric transition. Thus the defect (O^{2-} vacancy) probabilities P_i^V $(i=1-6)$ in the unaged ferroelectric state are the same at O^{2-} site 1–6 $(P_1^V=P_2^V=P_3^V=P_4^V=P_5^V=P_6^V)$, i.e., exhibiting a cubic defect symmetry [Fig. 7(a)]. As a result, for the unaged ferroelectric state cubic defect symmetry is inherited in the rhombohedral crystal symmetry [see the bottom illustration of Fig. 7(a)], but such a state is energetically unstable, according to the SC-SRO principle. For an acceptor-doped rhombohedral ferroelectric lattice, O^{2-} sites 1, 4, and 6 are closer to the acceptor ion D^{3+} than the other sites (2, 3, and 5) in distance; thus, they have larger probability to be occupied by oxygen vacancies due to the attractive Coulomb force between the effectively negative-charged D^{3+} dopant and the effectively positive-charged O^{2-} vacancy. Consequently the stable defect probability should be $P_1^V=P_4^V=P_6^V>P_2^V=P_3^V=P_5^V$, exhibiting a polar rhombohedral symmetry [Fig. 7(b)]. Consequently, again the stable defect symmetry follows the polar rhombohedral crystal symmetry, as suggested by SC-SRO principle. Apparently, the change from the unstable state [Fig. 7(a)] to the stable state [Fig. 7(b)] requires that is a short-range migration of O^{2-} vacancies and thus takes some time to complete. This is the origin of the aging in rhombohedral ferroelectrics, being the same as that in tetragonal ferroelectrics and orthorhombic ferroelectrics.

Similar to the case of tetragonal ferroelectrics and orthorhombic ferroelectrics, the polar rhombohedral defect symmetry in the aged rhombohedral ferroelectrics creates a defect polarization $\mathbf{P}_D$ aligning along $\mathbf{P}_S$ direction $\langle 111\rangle_{cub}$ [see the bottom illustration of Fig. 7(b)]. This defect polarization $\mathbf{P}_D$ provides a restoring force for a reversible domain switching like the case of tetragonal and orthorhombic ferroelectrics. Consequently a macroscopic double hysteresis loop and a large recoverable electrostrain behavior are also observed (Fig. 4). Clearly such a behavior is absent in unaged samples where the cubic defect symmetry cannot provide a restoring force.

In summary, based on the SC-SRO property of point defects, we provide a unified explanation for microscopic mechanisms of the aging effect in tetragonal, orthorhombic, and rhombohedral ferroelectrics, respectively. We show that ferroelectric aging originates from the inconformity of the defect symmetry with crystal symmetry after a structural transition. No matter what is the structure and/or symmetry of the crystal, point defects always try to rearrange to adopt the same SRO symmetry as the crystal symmetry, as stipulated by the SC-SRO principle. This is why aging is quite general and why it is not sensitively dependent on crystal structure and/or symmetry or ionic species, as shown in our

experiments with different crystal symmetries and ionic species.

Finally, it should be noted that the SC-SRO mechanism is akin to the dielectric relaxation mechanism suggested by Nowick and Heller.[28] Both can explain a relaxation of point defects after a perturbation, but with a difference that the former explains the relaxation after a change in crystal symmetry, whereas the latter explains the relaxation after a change in external field. SC-SRO mechanism is also related to the volume mechanism proposed by Lambeck and Jonker[6,21] and Robels and Arlt,[20] but with a difference in the driving force of the defect relaxation. In the SC-SRO mechanism the driving force for aging is the symmetry change; this makes it possible to explain aging in both ferroelectrics and in martensite.[8–13,22,23] However, the volume mechanism can explain the aging in ferroelectrics only because it relies on the existence of spontaneous polarization. Therefore, SC-SRO is a more general mechanism for aging.

V. CONCLUSIONS

We found striking similarity of aging effect (double a *P-E* hysteresis loop and a recoverable electrostrain behavior) in perovskite ferroelectrics with different crystal symmetries (tetragonal, orthorhombic, and rhombohedral) and ionic species. Such similarity in aging behavior for different crystal structures and ionic species suggests a common origin of aging. We show that aging originates from a general symmetry-conforming tendency of point defects, as stipulated by the SC-SRO principle. This explains why aging is not sensitively dependent on crystal symmetry or ionic species.

ACKNOWLEDGMENT

This work was supported by Kakenhi of JSPS.

[1] F. Jona and G. Shirane, *Ferroelectric Crystals* (Macmillan, New York, 1962).
[2] K. Okazaki, *Ceramic Engineering for Dielectrics* (Gakken-Shya, Tokyo, 1969).
[3] B. Jaffe, W. R. Cook, and H. Jaffe, *Piezoelectric Ceramics* (Academic, New York, 1971).
[4] K. Uchino, *Ferroelectric Device* (Dekker, New York, 2000).
[5] K. Carl and K. H. Hardtl, Ferroelectrics **17**, 473 (1978).
[6] P. V. Lambeck and G. H. Jonker, J. Phys. Chem. Solids **47**, 453 (1986).
[7] X. Dai, Z. Xu, and D. Viehlaud, J. Am. Ceram. Soc. **78**, 2815 (1995).
[8] X. Ren, Nat. Mater. **3**, 91 (2004).
[9] L. X. Zhang, W. Chen, and X. Ren, Appl. Phys. Lett. **85**, 5658 (2004).
[10] L. X. Zhang and X. Ren, Phys. Rev. B **71**, 174108 (2005).
[11] W. F. Liu, W. Chen, L. Yang, L. Zhang, Y. Wang, C. Zhou, S. T. Li, and X. Ren, Appl. Phys. Lett. **89**, 172908 (2006).
[12] L. X. Zhang and X. Ren, Phys. Rev. B **73**, 094121 (2006).
[13] Z. Feng and X. Ren, Appl. Phys. Lett. **91**, 032904 (2007).
[14] D. Damjanovic and M. Demartin, J. Phys.: Condens. Matter **9**, 4943 (1997).
[15] S. P. Li, W. W. Cao, and L. E. Cross, J. Appl. Phys. **69**, 7219 (1991).
[16] G. Arlt and U. Rebels, Integr. Ferroelectr. **3**, 343 (1993).
[17] D. A. Hall and M. M. Ben-Omran, J. Phys.: Condens. Matter **10**, 9129 (1998).
[18] K. Okasaki and K. Sakata, Electrotech. J. Jpn. **7**, 13 (1962).
[19] M. Takahashi, Jpn. J. Appl. Phys. **9**, 1236 (1970).
[20] U. Robels and G. Arlt, J. Appl. Phys. **73**, 3454 (1993).
[21] P. V. Lambeck and G. H. Jonker, Ferroelectrics **22**, 729 (1978).
[22] X. Ren and K. Otsuka, Nature (London) **389**, 579 (1997).
[23] X. Ren and K. Otsuka, Phys. Rev. Lett. **85**, 1016 (2000).
[24] M. Matsubara, K. Kikuta, and S. Hirano, J. Appl. Phys. **97**, 114105 (2005).
[25] W. C. Hahn and A. Muan, Am. J. Sci. **258**, 69 (1960).
[26] C. Klingsberg and R. Roy, J. Am. Ceram. Soc. **43**, 620 (1960).
[27] D. M. Smyth, *The Defect Chemistry of Metal Oxides* (Oxford University Press, New York, 2000).
[28] A. S. Nowick and W. R. Heller, Adv. Phys. **14**, 101 (1965).